

$\bar{p}p$ annihilation at rest into $K_L K^\pm \pi^\mp$

A. Abele, S. Bischoff, P. Blüm, N. Djaoshvili, D. Engelhardt, A. Herbstrith, C. Holtzhausen, and M. Tischhäuser
Universität Karlsruhe, D-76021 Karlsruhe, Germany

J. Adomeit, B. Kämmler, J. Meier, P. Schmidt, R. Seibert, and U. Strohbusch
Universität Hamburg, D-22761 Hamburg, Germany

C. Amsler, S. v. Dombrowski,* P. Giarritta, M. Heinzelmann, F. Ould-Saada, C. Pietra, C. Regenfus, and S. Spanier
Universität Zürich, CH-8057 Zürich, Switzerland

C. A. Baker, C. J. Batty, and C. N. Pinder
Rutherford Appleton Laboratory, Chilton, Didcot OX11 0QX, United Kingdom

B. M. Barnett, V. Credé, A. Ehmanns, M. Herz, H. Kalinowsky, E. Klempt, B. Pick, S. Resag, C. Strassburger, U. Thoma,
 and K. Wittmack
Universität Bonn, D-53115 Bonn, Germany

M. Benayoun
LPNHE Paris VI, VII, F-75252 Paris, France

A. Berdoz, R. McCrady, and C. A. Meyer
Carnegie Mellon University, Pittsburgh, Pennsylvania 15213

K. Beuchert, T. Degener, H. Koch, M. Kunze, U. Kurilla, J. Lüdemann, H. Matthäy, K. Peters, M. Ratajczak, and H. Stöck
Universität Bochum, D-44780 Bochum, Germany

K. Braune, O. Cramer, W. Dünnweber, M. A. Faessler, N. P. Hessey, D. Jannik,[†] C. Kolo, W. Roethel, C. Völcker,
 S. Wallis, D. Walther, U. Wiedner, and C. Zupančič
Universität München, D-80333 München, Germany

T. Case, K. M. Crowe, F. H. Heinsius,[‡] P. Kammel, and M. Lakata
University of California, LBNL, Berkeley, California 94720

M. Doser, J. Kisiel,[§] R. Landua, L. Montanet, and R. Ouaed
CERN, CH-1211 Geneva 4, Switzerland

R. P. Haddock
University of California, Los Angeles, California 90024

P. Hidas
Academy of Science, H-1525 Budapest, Hungary

M. Suffert
Centre de Recherches Nucléaires, F-67037 Strasbourg, France
 (Received 20 August 1997; published 27 February 1998)

We present a measurement and partial wave analysis of the final state $K_L K^\pm \pi^\mp$ of $\bar{p}p$ annihilation at rest in liquid hydrogen. This reaction is important for the study of the $\bar{K}K$ decay mode of scalar resonances, in particular, the isovectors $a_0(980)$ and $a_0(1450)$. The determination of the $a_0(1450)$ production also fixes the $\bar{K}K$ coupling of the isoscalar $f_0(1500)$ which is discussed as a glueball. We find $B(\bar{p}p \rightarrow a_0(1450)\pi; a_0(1450) \rightarrow \bar{K}K) = (8.88 \pm 1.68) \times 10^{-4}$ and hence $B(\bar{p}p \rightarrow f_0(1500)\pi; f_0(1500) \rightarrow \bar{K}K) = (4.52 \pm 0.36) \times 10^{-4}$. The mass and width of $a_0(1450)$ are $m = 1480 \pm 30 \text{ MeV}/c^2$ and $\Gamma = 265 \pm 15 \text{ MeV}/c^2$, respectively. For $a_0(980)$ we determine the relative ratio $B(\bar{p}p \rightarrow a_0\pi; a_0 \rightarrow \bar{K}K)/B(\bar{p}p \rightarrow a_0\pi; a_0 \rightarrow \pi\eta) = 0.23 \pm 0.05$ and its relative coupling, $\bar{K}K$ to $\pi\eta$, is 1.03 ± 0.14 . [S0556-2821(98)02907-5]

PACS number(s): 14.40.Ev, 13.25.-k, 14.40.Cs

*Now at Cornell University, Ithaca, New York 14853.

[†]Permanent address: University of Ljubljana, Ljubljana, Slovenia.

[‡]Now at University of Freiburg, Germany.

[§]Permanent address: University of Silesia, Katowice, Poland.

I. INTRODUCTION

Proton-antiproton annihilation at rest in liquid hydrogen is an excellent environment for the study of scalar meson resonances. The most sensitive channels consist of three neutral pseudoscalar mesons. The Crystal Barrel Collaboration has published the observation of an isovector scalar resonance $a_0(1450)$ with mass and width $m=1450\pm 40$ MeV and $\Gamma=270\pm 40$ MeV, respectively [1]. This state was required to describe the process $\bar{p}p\rightarrow\pi^0\pi^0\eta$. Recently, we have reported its $\pi^0\eta'$ decay [2] with a strength close to SU(3)-flavor expectations for a $\bar{q}q$ member of the scalar nonet. Information about a $\bar{K}K$ decay mode is still missing.

We have also published the observation of the $f_0(1500)$ resonance in its $\pi^0\pi^0$ [3], $\eta\eta$ [4], $\eta\eta'$ [5] and $4\pi^0$ [6] decay. We have established its couplings to $\pi\pi$, $\eta\eta$ and $\eta\eta'$ by performing a coupled channel analysis in the K-matrix formalism [7]. The $f_0(1500)$ is currently a good candidate for the ground state glueball, which is predicted in this mass range by lattice gauge theories [8]. Important for the understanding of its nature is its coupling to $\bar{K}K$. In a recent paper [9], we have shown evidence for its decay into $\bar{K}K$ in the reaction $\bar{p}p\rightarrow K_L K_L \pi^0$. In this channel the contributions from $f_0(1500)(I=0)$ and $a_0(1450)(I=1)$ decays to $K_L K_L$ cannot be disentangled. The $K_L K_L$ system carries isospin $I=0$ and $I=1$ allowing the occurrence of both of them. The partial wave analysis yielded a branching ratio $B(\bar{p}p\rightarrow\pi^0 f_0(1500); f_0(1500)\rightarrow\bar{K}K)$ ranging from $(3.9\pm 0.9)\times 10^{-4}$ to $(7.7\pm 1.6)\times 10^{-4}$ depending on the contribution from $a_0(1450)$ to $K_L K_L \pi^0$ (from 15 to 0%). In the reaction $\bar{p}p\rightarrow K_L K^\pm \pi^\mp$ only the $I=1\bar{K}K$ resonances are produced with fractional contributions κ^\pm and, if interferences with other resonances are neglected, their intensities in the $K_L K_L \pi^0$ final state κ^0 may be calculated by applying isospin symmetry:

$$\kappa^0 = \frac{B(K_L K^\pm \pi^\mp)}{4B(K_L K_L \pi^0)} \kappa^\pm. \quad (1)$$

In this paper we describe the selection of the final state $K_L K^\pm \pi^\mp$ from $\bar{p}p$ annihilation at rest in liquid hydrogen and a partial wave analysis in the K-matrix formalism.

II. DATA SELECTION

The Crystal Barrel experiment used antiprotons from the Low Energy Antiproton Ring (LEAR) at CERN. The detector started operating in 1989 and finished data taking with the shutdown of LEAR in 1996. Final states from antiproton-proton annihilation consist mainly of charged pions and kaons, together with photons originating mostly from the decay of short lived particles such as π^0 , η and ω . The Crystal Barrel spectrometer was constructed for the detection of charged and neutral decay products with a solid angle of 97% of 4π . Antiprotons with a momentum of 200 MeV/c and an incident rate of at most 30 kHz were stopped in the center of a liquid hydrogen target. The whole detector assembly was placed in a solenoidal magnetic field of 1.5 T for momentum analysis of the charged annihilation products:

two concentric cylindrical multiwire proportional chambers allowed a fast decision on the charged particle multiplicity. They were surrounded by a cylindrical jet drift chamber (JDC), which was divided into 30 sectors, each containing 23 sense wires with a spatial resolution of $\sigma=125\ \mu\text{m}$ in (r ϕ) and $\sigma=7$ mm for the z coordinate. The measured momentum resolution for a long track reaching the outer layers of the JDC was 2% at 200 MeV/c and about 7% at 1 GeV/c. From the pulse heights on all wires along a track, information on the dE/dx for particle identification was obtained. A barrel shaped electromagnetic calorimeter segmented into 1380 CsI(Tl) crystals, 16.1 radiation lengths deep, surrounded the JDC. The crystals were read out with photodiodes. A detailed description of the detector can be found in Ref. [10].

The $K_L K^\pm \pi^\mp$ final state was reconstructed by requiring a missing K_L and two charged particles [11]. The candidate events are characterized by two long, oppositely curved tracks starting in the liquid hydrogen target and reaching the calorimeter. Due to its long lifetime, a K_L with a typical momentum of 400 MeV/c reaches the CsI barrel (average distance 0.4 m from the target) with a probability of 96.8%. In $(54\pm 4)\%$ of all cases it initiates a detectable shower near its impact point. The pattern of the energy deposition in the crystals is difficult to distinguish from that of a photon from π^0 or η decay. To suppress background from channels like $\pi^+\pi^-\pi^0$ and $\pi^+\pi^-\eta$ which have a higher branching ratio than $K_L K^\pm \pi^\mp$, and since the probability to miss two photons is rather small, we keep only events with a missing mass of the K_L .

The analysis is based on 7.7 million events triggered by two long charged tracks, allowing any multiplicity of distinct energy depositions in the calorimeter. The enrichment factor of the signal channel in this sample is about 7 compared to minimum bias data. The off-line criteria for long tracks are signals in the inner and the outer sense wire layers of the JDC, at least 10 hits and a satisfactory helix fit to the space points. This reduces the data sample to 5.6 million good two prong events with long tracks. The threshold for a particle energy deposition in the calorimeter is set to 10 MeV. An energy deposition found close to the impact point of a track is not counted as decay photon or interacting K_L unless it can be combined to a π^0 or η with a second energy cluster. We obtained a sample of 132846 events with two long tracks and no additional electromagnetic shower.

Assuming that both charged particles are pions we show their missing mass in Fig. 1. One expects the peak of the missing K_L to be centered at 728 MeV/c², where a clear signal from K_L is observed. In addition one sees the collinear ($\pi^+\pi^-$, K^+K^-) and $\pi^+\pi^-K_L K_L$ events with both K_L not detected. With the fit of a Gaussian plus a straight line to the signal we estimate 12000 ± 600 $K_L K^\pm \pi^\mp$ events. In Fig. 2 the total momentum is plotted versus the total energy for all 132846 events. In the region marked (A) one expects collinear events. The signal events are seen in the band labeled (B). It spans the allowed K_L momentum range up to 747 MeV/c. The plot is also populated with $K_S K_L$ events, K_S decaying into $\pi^+\pi^-$ and K_L missing, [region (C)], and $\pi^+\pi^-K_L K_L$ events [area (D)]. In region (E) $\bar{p}p\rightarrow\pi^+\pi^-\pi^0$ events show up where the two decay photons of the π^0 were not detected. The final states $\pi^+\pi^-\pi^0$, $K_S K_L$

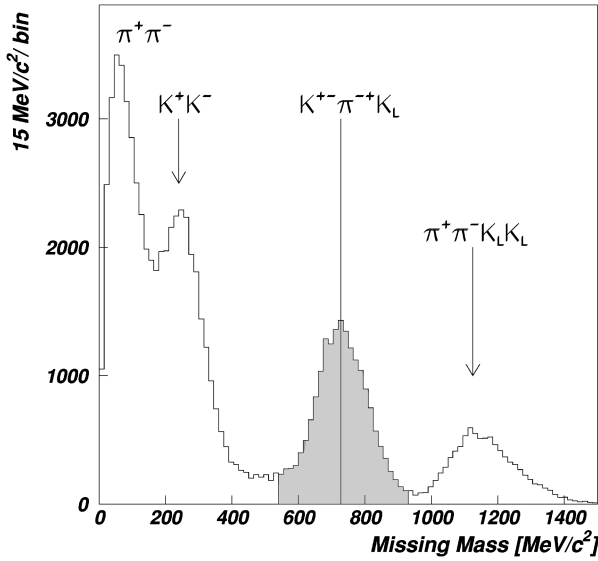


FIG. 1. Two-prong missing mass with no additional energy cluster, assuming pions.

and K^+K^- appear in the kinematic neighborhood of $K_L K^\pm \pi^\mp$ and can therefore contribute to the background.

At this stage we take events from the shaded area in Fig. 1 and accept those with a missing $K^+ \pi^-$ or $K^- \pi^+$ mass in the window:

$$350 \text{ MeV}/c^2 < \text{missing mass}(K^+ \pi^- \text{ or } \pi^+ K^-) < 650 \text{ MeV}/c^2 \quad (2)$$

and if it lies in region (B) in Fig. 2 which is kinematically well separated from other channels, we arrive at 17265 events. We can easily distinguish $K_S K_L$ events leaking into region (B) from our signal events since the average decay length of the K_S is 4.3 cm, leading to a secondary vertex which lies outside the target region ($r=1.2$ cm). We keep

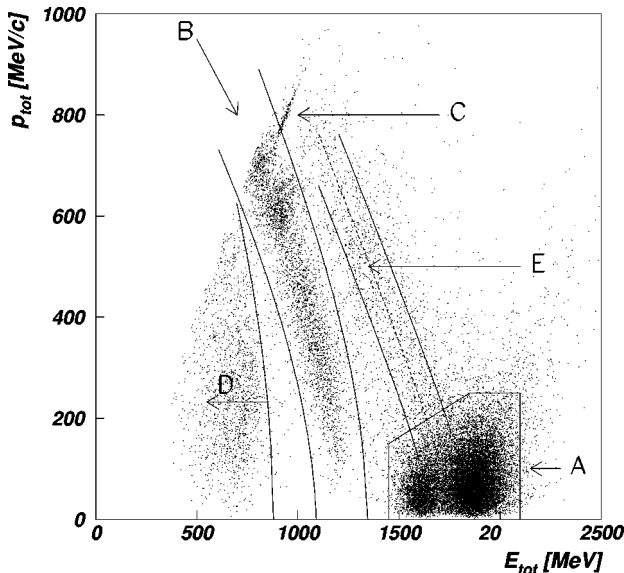


FIG. 2. Total energy versus total momentum. For the calculation of the energy all charged particles are assumed to be pions (see text). Region (B) corresponds to $K_L K^\pm \pi^\mp$ events.

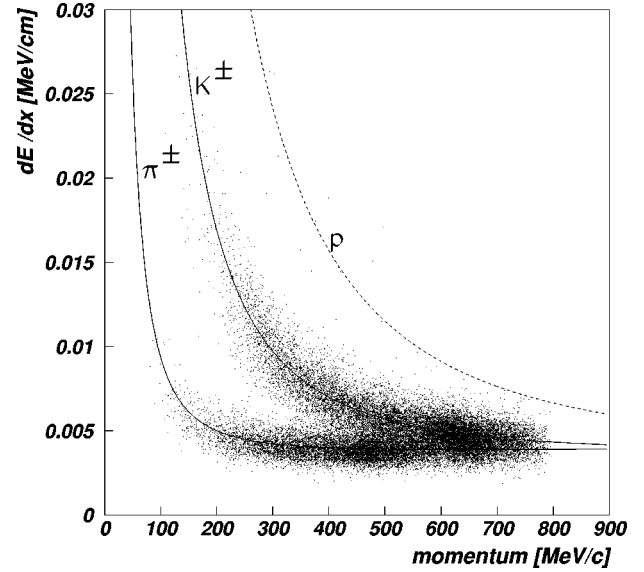


FIG. 3. dE/dx distribution for all 17208 events with an entry in the missing mass window.

17208 events from region (B). According to Monte Carlo simulation we are then left with less than 20 $K_S K_L$ events. Further background subtraction will be discussed below.

As shown, topology and kinematic cuts already define the $K_L K^\pm \pi^\mp$ final state rather well. The next step is to separate $K_L K^\pm \pi^\mp$ from $K_L K^- \pi^+$ by dE/dx and both from the remaining $K^+ K^- X$ and $\pi^+ \pi^- X$ events with X decaying into undetected particles. The dE/dx distribution versus particle momentum is shown in Fig. 3. The maximum momentum of charged particles is below 800 MeV/c. Therefore, a simplified Bethe-Bloch formula is used:

$$-dE/dx^{theo} = \frac{M}{\beta^2} \left[\ln \left(N \frac{\beta^2}{1-\beta^2} \right) - \beta^2 \right]. \quad (3)$$

The constants M, N were adjusted to a $\pi^+ \pi^- \pi^0$ and $K^+ K^- \pi^0$ sample using the truncated mean method—the lowest 10% and highest 30% of dE/dx values are rejected. From a fit of Gaussians to the dE/dx distributions of π and K in different momentum intervals we derive a resolution of $\sigma(dE/dx) = 0.142 \times dE/dx$, enabling a (3σ) π/K separation up to 470 MeV/c.

The different hypotheses are distinguished by a χ^2 test:

$$\chi_{ij}^2 = \chi_i^2 + \chi_j^2, \quad (4)$$

where

$$\chi_i^2 = \left(\frac{dE/dx_i^{theo} - dE/dx_i}{\sigma_i(dE/dx)} \right)^2, \quad (5)$$

and i, j stands for a π or a K . The lowest of the four possible values χ_{ij}^2 determines our particle assignment. By this method we select 6240 $K_L K^+ \pi^-$ and 6430 $K_L K^- \pi^+$ events. In only 2% of all cases does the assignment to one of the signal channels from dE/dx contradict the classification based on the missing mass equation (2). These events were rejected. We expect a slightly enhanced efficiency for the K^- mode, since a low momentum K^- ($p < 250$ MeV/c) fires

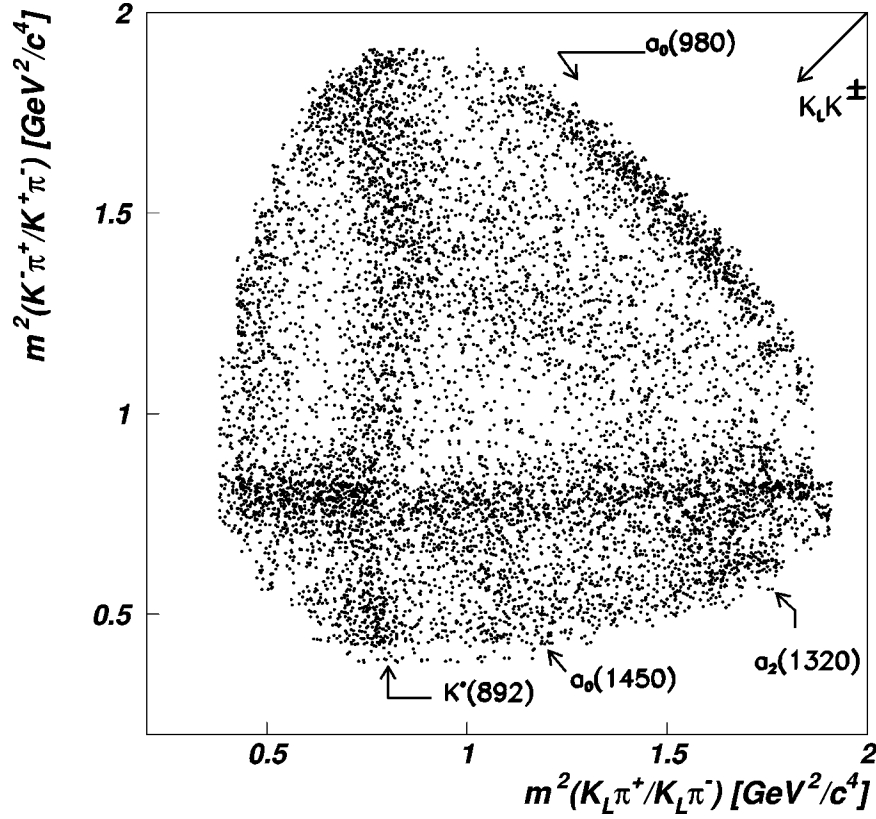


FIG. 4. Acceptance corrected and background subtracted $K_L K^\pm \pi^\mp$ Dalitz plot. The plot is divided into quadratic cells of size $0.045 \times 0.045 \text{ GeV}^4/c^2$. The dots represent the event density.

more crystals than a K^+ and hence has a higher track matching probability. The events are then kinematically corrected for energy and momentum conservation with the hypothesis of a missing K_L (1C-fit). Events with a confidence level greater than 10% are accepted leading to $11373 K_L K^\pm \pi^\mp$ events. Fig. 4 shows the $K_L K^\pm \pi^\mp$ Dalitz plot, already corrected for acceptance and with background subtracted, as discussed in the following.

The detection and reconstruction efficiency ϵ^\pm for two charged tracks ($\pi^\pm K^\mp$) and the missing K_L was determined by a Monte Carlo simulation of the complete detector based on GEANT [12]. To simulate hadronic interactions we used the FLUKA package [13]. We explicitly extract the K_L interaction probability from data according to Ref. [9]. The average interaction probability is $P^{int} = (54 \pm 4)\%$. The momentum dependence is as follows:

$$P^{int} = A + (1 - A) \exp\left(-\frac{p}{B}\right), \quad (6)$$

with $A = 0.50 \pm 0.01$ and $B = (145 \pm 28) \text{ MeV}/c$. The parametrization accommodates the measurement at a K_L momentum of $795 \text{ MeV}/c$ in the channel $\bar{p}p \rightarrow K_L K_S$ at rest: $P^{int} = (57.2 \pm 2.7)\%$ [14]. We also have to correct for a K_L induced shower in the calorimeter which is hidden in a cluster assigned to a charged pion or kaon. This effect is expected to be enhanced at the $\bar{K}K$ threshold (when the K_L and K^\pm momenta are parallel) and in the region where the K_L and the charged pion move parallel. The simulation tool [13] provides cross sections for K_L only for momenta above

$230 \text{ MeV}/c$. The range below $230 \text{ MeV}/c$ covers only a small fraction of our sample. To determine the correction to the acceptance ϵ^\pm in our channel down to lower momenta we established the pattern of K_L energy clusters in CsI(Tl) using the annihilation channel $K_L K_S \pi^0$ with $K_S \rightarrow \pi^+ \pi^-$. From 3.36 million events triggered by a secondary vertex and two charged tracks we selected 5323 events by applying the following main selection criteria: the $\pi^+ \pi^-$ invariant mass had to match the K_S mass, the two photons found could be combined to a π^0 and the missing $K_S \pi^0$ mass lies in a window around the K_L mass. The π^+ , π^- and the photons were not allowed to fly in the direction of the K_L . In the K_L momentum range up to $230 \text{ MeV}/c$ we did not find significant differences in the pattern of energy deposition compared to the interval 230 to $330 \text{ MeV}/c$. From the Monte Carlo simulation of events with K_L interacting we derived a correction factor for the hidden K_L . Combining this with the reconstruction efficiency ϵ^\pm for the two charged particles we arrived at an average efficiency of $\epsilon = (14.9 \pm 0.1_{stat} \pm 0.5_{sys})\%$.

The branching ratio is calculated with 1 million minimum bias events. We find 213 ± 15 events surviving our selection chain. With the reconstruction efficiency ϵ and the average non-interaction probability $\bar{P}^{int} = (46 \pm 4)\%$ we arrive at the branching ratio:

$$B(K_L K^\pm \pi^\mp) = (2.91 \pm 0.34) \times 10^{-3}. \quad (7)$$

This value agrees within 2σ with that for the channel $K_S K^\pm \pi^\mp$ of Armenteros *et al.* [15] ($B(K_S K^\pm \pi^\mp) = (2.82$

$\pm 0.11) \times 10^{-3}$) and Barash *et al.* [16] ($\frac{1}{2}B(K^0 K^\pm \pi^\mp) = (2.13 \pm 0.28) \times 10^{-3}$). We have more than five times higher statistics but the largest contribution to our error originates from the uncertainty in the K_L interaction probability. For the normalization of the partial branching ratios in our Dalitz plot analysis we take the average of the branching ratios from the bubble chambers [15,16] and this analysis:

$$B(\bar{p}p \rightarrow K_L K^\pm \pi^\mp) = (2.74 \pm 0.10) \times 10^{-3}. \quad (8)$$

Low momentum pions and kaons ($p \leq 50$ MeV/c) curl in the JDC. For this small fraction of events the acceptance drops to zero. Slow charged kaons from our signal channel may already stop in the liquid hydrogen target and decay into $\mu^\pm \nu_\mu$. By dE/dx the μ is not distinguishable from a π . A fast π ($p > 500$ MeV/c), on the other hand, can be misidentified as a kaon, simulating $K_L K^\pm \pi^\mp$ events at $\bar{K}K$ masses around 1580 MeV/c². One expects, however, only 15 ± 4 events of this kind. High momentum charged π and K cannot be separated by dE/dx anymore and may lead to wrong $K^+ \pi^- / K^- \pi^+$ combinations. According to Monte Carlo simulation this happens only for a small fraction of the selected $K_L K^\pm \pi^\mp$ events ($0.75 \pm 0.05\%$).

We have generated possible background channels with the full detector Monte Carlo and subjected the events to the same reconstruction chain as the data. From the number of events surviving the selection and the branching ratios of the relevant channels one can calculate the effective number of background events in the $K_L K^\pm \pi^\mp$ final state. The most important candidate is the $\pi^+ \pi^- \pi^0$ channel with its high branching ratio of $(6.6 \pm 0.8)\%$ [17] even though the two-photon escape probability is only about 0.1%. These events originate from a depopulated region of the $\pi^+ \pi^- \pi^0$ Dalitz plot and contribute to $K_L K^\pm \pi^\mp$ with (60 ± 16) events while $\pi^+ \pi^- \eta$ contributes (47 ± 10) events. Furthermore, we found $(28 \pm 9) K^+ K^- \pi^0$ events (2 γ missed detection and one fast K simulates a π), $(27 \pm 4) K^+ K^-$ events (a fast K is misidentified and the mass difference between K and π is attributed to the missing K_L), $(18 \pm 3) K_S K_L$ events and $(10 \pm 4) \pi^+ \pi^- \omega$ events (3 photons are not detected). There is practically no contamination from the four-body channel $K_L K_L \pi^+ \pi^-$. The total fraction of background events in the signal channel is $(1.7^{+1.7}_{-0.7})\%$. The systematic error on this number is already included and was established by varying the charged momentum and dE/dx calibration of the JDC within the error range of calibration constants. The background is found at low $K_L \pi^\pm$ masses at the left border of the $K_L K^\pm \pi^\mp$ Dalitz plot (see Fig. 4). For the Dalitz plot analysis they have been subtracted. As an additional test in the partial wave analysis a background Dalitz plot was incoherently added to the simulated intensity distribution and its strength determined by a fit to a value of less than 2%.

III. DALITZ PLOT ANALYSIS

In the Dalitz plot the two body systems with isospin $I = \frac{1}{2}(K^\pm \pi^\mp, K_L \pi^\pm)$ are seen along horizontal and vertical straight lines, respectively. The charged $I = 1(K_L K^\pm)$ system is seen along the diagonal axis. We observe two resonance bands crossing each other at low $K\pi$ masses. They belong to

the $K^{*\pm}(892)$ and $K^{*0}(892)$. Isospin interferences cause an asymmetric population of the bands. One also sees the $a_0(980)$ as a strong enhancement at the $\bar{K}K$ threshold. The $a_2(1320)$ appears at the edges and in the middle of the plot. This is typical for a spin-2 resonance produced from initial S states. In the bubble chamber analysis the $a_2(1320)$ mass position was determined to be $m = 1280$ MeV/c² [18,19]. We shall see that this shift compared to the Particle Data Group (PDG) [20] mass value of 1320 MeV/c² is explained by the introduction of a further scalar resonance, $a_0(1450)$. The impression of a curved $K^{*\pm}(892)$ band is created by the interference with the $a_2(1320)$.

We now describe the partial wave analysis. Proton and antiproton couple to isospin $I_{pp}^- = 0$ and 1. For annihilation at rest in liquid hydrogen the dominant contribution stems from the initial protonium S states: $^1S_0(J^{PC} = 0^{-+})$ and $^3S_1(J^{PC} = 1^{--})$ [21]. A detailed analysis including annihilation from P states is not possible because of the disproportionate increase in the number of parameters. At low energy the intermediate meson resonances carry spin 0, 1 or 2. For $K_L K^\pm \pi^\mp$ the $K^{*\pm}(892)$ and $K^{*0}(892)$ bands interfere constructively for $I=0$ and destructively for $I=1$ (while for $K^+ K^- \pi^0$ and $\bar{K}^0 K^0 \pi^0$ the interference is always constructive). The simulation of the two $K^*(892)$ transitions from 1S_0 and 3S_1 are shown as intensity plots in Figs. 5(g,h) and Fig. 5(k,l), respectively. The transitions from the same initial state add coherently with relative strengths and production phases which can be determined by a partial wave analysis. Different initial states add incoherently.

The total transition amplitude factorizes into a dynamical part F_l , commonly parametrized in terms of a relativistic Breit-Wigner formula, a spin-parity function calculated in helicity formalism [22] and a damping form factor taken usually from Refs. [23,24] and depending on the decay angular momentum. The analytic form and conservation of unitarity is ensured by replacing the relativistic Breit-Wigner amplitudes by the more general ansatz [24]:

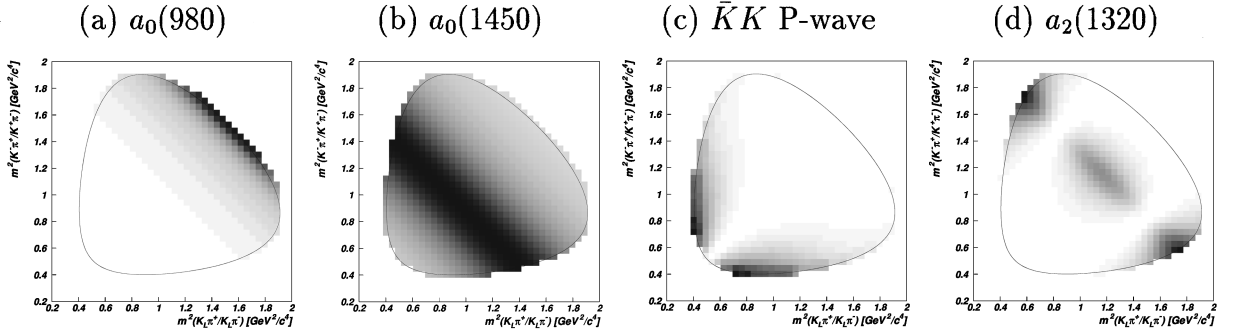
$$F_l = (1 - iK_l \rho)^{-1} P_l, \quad (9)$$

which reduces to a Breit-Wigner expression in the simple case of a single resonance in a given partial wave l with only one decay channel open. F_l and P_l are vectors, K_l , ρ and $\mathbb{1}$ are matrices. In the following we omit the index l labeling different partial waves. In the Lorentz invariant K-matrix K we include the resonance singularities by a simple sum of poles m_α , which, in general, do not coincide with the physical resonance masses and widths. These have to be extracted as poles of the function F in the complex energy plane [24]. The general form of the K matrix for the propagation of a two-body channel i into a channel j through the resonances α with real couplings $g_{\alpha i}$ and $g_{\alpha j}$ is given by:

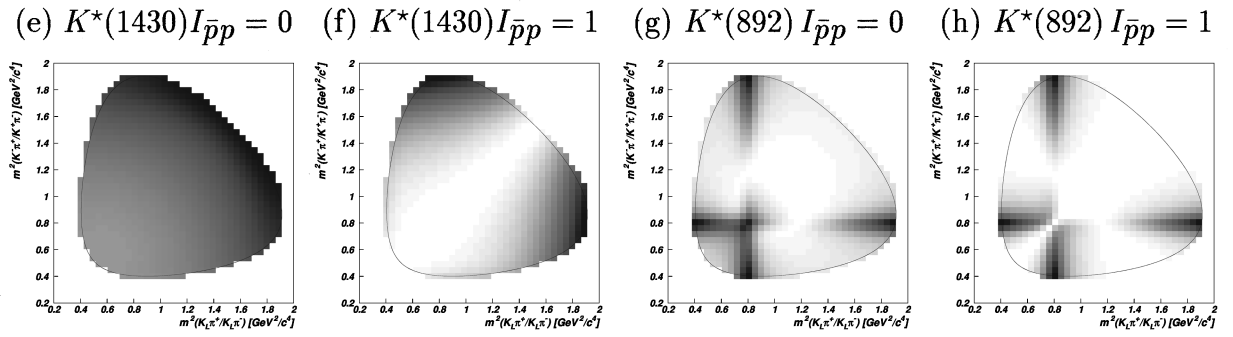
$$K_{ij}(m) = \sum_\alpha \frac{g_{\alpha i} g_{\alpha j}}{m_\alpha^2 - m^2} \frac{B_l(q_i)}{B_l(q_{\alpha i})} \frac{B_l(q_j)}{B_l(q_{\alpha j})}, \quad (10)$$

with $q_i = q_i(m)$, the breakup momentum for the decay into a given two-body channel i . The phase space ρ_i is given by $\rho_i(m) = 2q_i/m$. The couplings $g_{\alpha i} = g_i(m_\alpha)$ of the pole α to channel i are related to the partial widths $\Gamma_{\alpha i}$ via

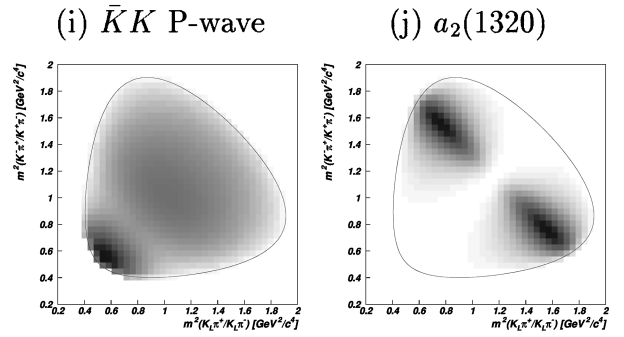
1S_0 $A(\bar{p}p \rightarrow R\pi \rightarrow \bar{K}K\pi)$



1S_0 $A(\bar{p}p \rightarrow RK \rightarrow \bar{K}K\pi)$



3S_1 $A(\bar{p}p \rightarrow R\pi \rightarrow \bar{K}K\pi)$



3S_1 $A(\bar{p}p \rightarrow RK \rightarrow \bar{K}K\pi)$

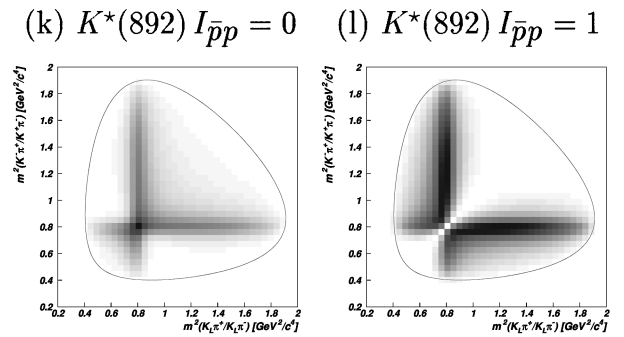


FIG. 5. Simulated intensity distributions of contributive partial waves.

$$g_{ai}^2 = \frac{m_\alpha \Gamma_{ai}}{\rho_i(m_\alpha)}. \quad (11)$$

The factors $B_l(q_i)$ are the damping factors [23,24]. The total width Γ_α is the sum of the partial widths divided by phase space evaluated at m_α . Equation (9) is derived from the expression for two-body scattering, which is described by the transition matrix T :

$$T_l = (1 - iK_l \rho)^{-1} K_l. \quad (12)$$

For production the annihilation vertex of the $\bar{p}p$ system is described by a complex coupling β'_α replacing one g_{ai} in the K matrix:

$$\beta_\alpha = \frac{\beta'_\alpha}{\sqrt{\sum_i g_{ai}^2}} = a_\alpha \exp(i\phi_\alpha), \quad (13)$$

and so

$$P_i = \sum_\alpha \frac{\beta'_\alpha g_{ai}}{m_\alpha^2 - m^2} \frac{B_l(q_i)}{B_l(q_{ai})}. \quad (14)$$

The expressions (9) and (12) both involve the K matrix and directly relate resonance production in two-body scattering and $\bar{p}p$ annihilation. Equations (8)–(13) may be considered as a concise formulation of the isobar model for protonium annihilation into three mesons via two-meson intermediate resonances. The free parameters are the masses m_α , couplings g_{ai} and $\beta_\alpha(a_\alpha, \phi_\alpha)$ of the resonance contributions. One phase per initial state is set to zero since it is not observable.

The total transition amplitude squared describes the event density N_i^{theo} at each position i of the three-body phase space. The Dalitz plot is fitted using the χ^2 -minimization method based on the MINUIT [25] program package. The χ^2 for a Poisson process is formulated as in Ref. [26]:

$$\chi^2 = 2 \sum_i [y_i - n_i + n_i \ln(n_i/y_i)], \quad (15)$$

with n_i the number of events in the i th Dalitz plot bin and y_i the number of events predicted by the model in the i th bin. Neglecting bins at the Dalitz plot boundary, 730 cells enter the calculation. The transition amplitude for a partial wave l squared and integrated over phase space gives its fractional contribution in the absence of interferences between various chains. Hence, in general, the sum of the individual contributions is not equal to 1.

We now present the first fit based on well established resonances only. The $K^*(892)$ resonance is parametrized as a relativistic Breit-Wigner amplitude since only the $K\pi$ channel is open. The charged $K^{*\pm}$ mass is found in all fits with the stable position $m_0 = (891 \pm 3) \text{ MeV}/c^2$ and $\Gamma_0 = (61 \pm 3) \text{ MeV}/c^2$. The freely fitted mass difference between K^{*0} and $K^{*\pm}$ is $\Delta m = (7 \pm 2) \text{ MeV}/c^2$. The width is affected by the mass resolution $\sigma_m = 12 \text{ MeV}/c^2$ at the K^* mass, according to simulation. Replacing the Breit-Wigner by the folding of a Breit-Wigner and a Gaussian (Voigtian

function) gives a resonance width of $m = (52 \pm 3) \text{ MeV}/c^2$. The parameters agree well with measurements of other experiments in Ref. [20].

The enhancement at the $\bar{K}K$ threshold (Fig. 4) is generated by the $a_0(980)$ resonance which couples to $\pi\eta$ and $\bar{K}K$. Therefore, it is parametrized by a 2×2 K matrix reducing to the well known Flatté formula [27]:

$$F_0 = \beta'_0 \frac{\begin{pmatrix} g_1 \\ g_2 \end{pmatrix}}{m_0^2 - m^2 - i(\rho_1 g_1^2 + \rho_2 g_2^2)}. \quad (16)$$

It was previously used in the analysis of the $\pi^0\pi^0\eta$ Dalitz plot [1,28] for which $g_1 = g_{\pi\eta}$ was determined to be $g_1 = 353 \text{ MeV}$. There the information about the two couplings in the $\pi\eta$ channel was extracted from the cusp-like shape of the $\pi\eta$ intensity which is caused by the opening of the $\bar{K}K$ threshold and introduces a correlation between the couplings.

For the $a_2(1320)$ we used a relativistic Breit-Wigner amplitude. It can be produced from the $(I=0)^1S_0\bar{p}p$ initial state—the angular distributions has a W shape—and the $(I=1)^3S_1$ initial state—a U-shaped angular distribution peaking at the Dalitz plot boundary [see Figs. 5(d) and 5(j)].

In addition to the $K\pi$ P wave we expect a $I=\frac{1}{2}$ S wave which contains the $K^*(1430)$. The parameters of the $K\pi$ S wave were determined by fitting a scattering amplitude $T = (1/\rho)\sin\delta e^{i\delta}$, Eq. (12) based on the K matrix to the phase shift of the LASS experiment [29]. It is purely elastic in the region of interest. We used the following ansatz:

$$K = \frac{g_0^2}{m_0^2 - m^2} + c_1 + c_2 m. \quad (17)$$

This form also includes the low-energy ($K\pi$) scattering. The fit yielded the constants $c_1 = 1.45$ and $c_2 = -0.55/\text{GeV}$ and $m_0 = (1342 \pm 10) \text{ MeV}/c^2$, $\Gamma_0 = (400 \pm 20) \text{ MeV}/c^2$. The resonance mass and width extracted from the T matrix in the complex energy plane are $m = (1428 \pm 10) \text{ MeV}/c^2$ and $\Gamma = (280 \pm 15) \text{ MeV}/c^2$, in close agreement with LASS [29]. In the Dalitz plot analysis using Eq. (9) these values were then fixed. Alternatively, the K matrix was formulated in terms of a scattering length including one resonance pole:

$$K = \frac{am}{2 + abq^2} + \frac{g_0^2}{m_0^2 - m^2} \quad (18)$$

with a the scattering length and b the effective range. A fit of this form gives $a = (2.58 \pm 0.21) \text{ GeV}^{-1}$ and $b = (1.81 \pm 0.25) \text{ GeV}^{-1}$. The K-matrix values (m_0, Γ_0) and the T-matrix pole are, within errors, the same as before. For the transition from the $I=1$ 1S_0 state one obtains destructive interference between the two charges; from 1S_0 $I=0$ the interference is constructive. The fit to the data shows that the pole term in the K matrix is the dominant part. The $I=1$ 1S_0 initial state can also decay via the $I=\frac{3}{2}$ $K\pi$ S wave. So far no resonance has been observed in this system [20]. If the $I=\frac{3}{2}$ wave has a similar energy dependence as the $I=\frac{1}{2}$ wave, they cannot be distinguished in the $K^0 K^\pm \pi^\mp$ final state. Hence we refrain from including it.

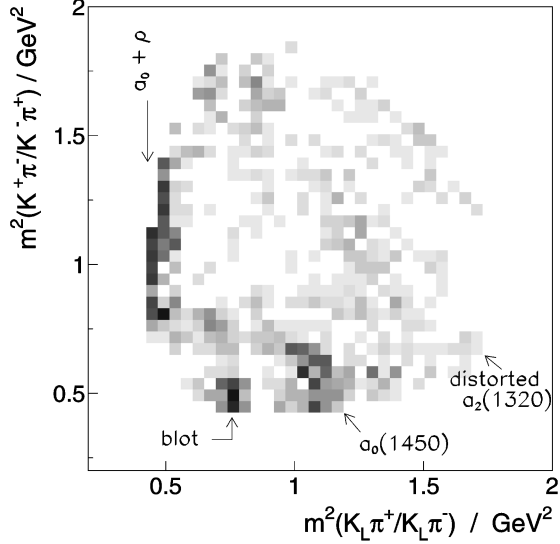


FIG. 6. Discrepancy over the Dalitz plot for the minimum hypothesis. The marked features are the lack of predicted intensity at low $K\pi$ masses and at the $a_0(1450)$ position, the distorted $a_2(1320)$ band and the blot in the $K^{*\pm}(892)$ band.

With this minimal hypothesis requiring 29 free parameters the fit leads to a $\chi^2/N_{dof} = 1380/(730-29)$. It is not a satisfactory description since systematic deviations between theory and data are observed in the Dalitz plot. In particular, the region for $\bar{K}K$ masses above the $a_2(1320)$ band is not described properly, as can be seen by the discrepancy between predicted events and data in Fig. 6. The $a_2(1320)$ mass position tends to a value below $1300 \text{ MeV}/c^2$. This phenomenon was already observed in the bubble chamber analyses [19,16].

In the next step we introduce a pole for the $a_0(1450)$ in the 2×2 K matrix in addition to $a_0(980)$. Since the $\pi\eta$ and $\bar{K}K$ thresholds are far away they do not significantly influence the line shape of the $a_0(1450)$ and therefore it suffices to consider the $\bar{K}K$ coupling of this resonance. The quality of the description improves significantly to $\chi^2/N_{dof} = 969/(730-33)$. Two aspects give further confidence in the introduction of this resonance: First, the $a_2(1320)$ is now found at a mass of $m = 1312 \pm 5 \text{ MeV}/c^2$ and with a width of $\Gamma = 117 \pm 5 \text{ MeV}/c^2$, in good agreement with our analysis of the $\pi^0\pi^0\eta$ final state. Secondly, the mass and width of the $a_0(1450)$ are fitted to $m = 1489 \pm 10 \text{ MeV}/c^2$ and $\Gamma = 265 \pm 11 \text{ MeV}/c^2$, respectively. This agrees with the analysis of $\pi^0\pi^0\eta$ in Refs. [1, 28]. For the 1S_0 initial state, the strength of $a_2(1320)$ is correlated with the strength of $a_0(1450)$: for an $a_2(1320)$ contribution increasing from 11% to 15% the $a_0(1450)$ increases from 8% to 13% while χ^2 increases by about $\Delta\chi^2 = 10$, at most.

We are left with a discrepancy in Fig. 6 evidenced by the blot in the $K^{*\pm}$ band at low $K^\pm\pi^\mp$ masses (see χ^2 distribution, Fig. 7). The interference between the K^* bands does not explain all of the observed intensity. The difference could be due to a resonance in the $\bar{K}K$ system at high mass which runs through the K^* band. The maximum intensity close to the Dalitz plot edge suggests a resonance with non-zero spin. A candidate is the radial excitation of the $a_2(1320)$, the

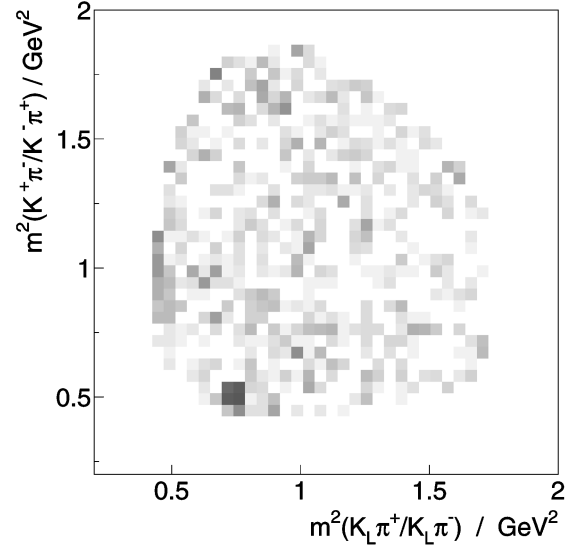


FIG. 7. χ^2 distribution over the Dalitz plot after inclusion of $a_0(1450)$.

$a_2(1650)$, which was already introduced in $\pi^0\pi^0\eta$ in Ref. [1]. The fit to $K_L K^\pm \pi^\mp$ accepts the additional pole in the $\bar{K}K$ D-wave with an improvement in the χ^2 of 50, although the width takes unreasonable values below $50 \text{ MeV}/c^2$. Also, one expects suppression of a spin-2 resonance close to the end of phase space ($m = 1740 \text{ MeV}/c^2$) due to the centrifugal barrier in the production. With spin 1 instead, the mass position decreases to about $1600 \text{ MeV}/c^2$ and the width becomes $\Gamma \approx 200 \text{ MeV}/c^2$. The χ^2 decreases significantly by $\Delta\chi^2 = 160$ and the blot is now described satisfactorily. The χ^2 distribution is shown in Fig. 8.

The observation of a vector meson with a mass above $1400 \text{ MeV}/c^2$ decaying into $\bar{K}K$ was reported [30] in the reaction $\pi^\pm p \rightarrow K_S K^\pm p$ at $30 \text{ GeV}/c$ and $50 \text{ GeV}/c$. Two radial excitations of the $\rho(770)$ are known [20], the $\rho(1450)$ and the $\rho(1700)$. These resonances were also reported by our

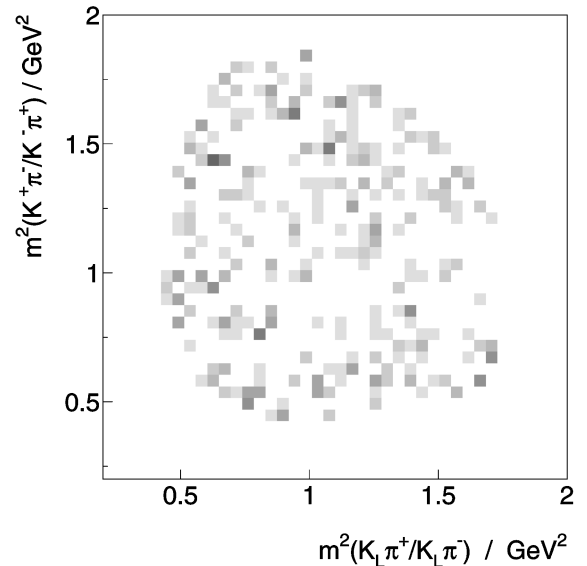


FIG. 8. χ^2 distribution over the Dalitz plot for the best hypothesis is flat. The scaling of blackness is the same as in Fig. 6.

TABLE I. Resonance contributions and relative production phases. A negative a_α means a phase offset of π .

Resonance	$I(\bar{p}p)$	Relative intensity [%]	a_α	ϕ_α [rad]
1S_0		62±5		
$K^*(892)$	0	7.5±1.0	-1.45	0.0
	1	1.1±0.4	0.64	3.9
$K\pi$ S-wave	0	30.3±7.0	-2.49	6.0
	1	4.7±2.0	3.45	5.5
$a_0(980)$	0	7.2 $^{+0.5}_{-1.2}$	12.53	0.4
$a_0(1450)$	0	10.8±2.0	1.27	4.6
$\bar{K}K$ P-wave	1	3.2 $^{+0.5}_{-1.0}$	0.60/1.72	3.8/5.9
$a_2(1320)$	0	14.6 $^{+1.0}_{-3.0}$	2.30	4.3
Sum		79.4±8.0		
3S_1		38±4		
$K^*(892)$	0	5.5±1.5	0.87	0.0
	1	20.2±3.0	1.97	5.3
$\bar{K}K$ P-wave	0	3.2±1.0	-0.4/1.3	0.1/2.2
$a_2(1320)$	1	5.2±1.6	1.10	5.4
Sum		34.1±3.8		
Total sum		113.5±8.9		

collaboration, decaying to $\pi^-\pi^0$ in $\bar{p}n \rightarrow \pi^-\pi^0\pi^0$ in liquid deuterium [31]. We therefore tried a two-pole K matrix for the $\bar{K}K$ P wave, $(m_\alpha, \Gamma_\alpha) = (1430 \text{ MeV}/c^2, 170 \text{ MeV}/c^2)$ and $(1740 \text{ MeV}/c^2, 190 \text{ MeV}/c^2)$, which reproduce the T-matrix poles for $\rho(1450)$ and $\rho(1700)$ in Ref. [20]. This does not change the situation in the Dalitz plot since both poles add to a single resonance peak around $1600 \text{ MeV}/c^2$ by appropriate choice of the production strengths and phases. The χ^2 for this best fit is $\chi^2/N_{\text{dof}} = 810/(730-45)$. In this fit the mass of the $a_0(1450)$ can be moved between $1450 \text{ MeV}/c^2$ and $1510 \text{ MeV}/c^2$ changing χ^2 by only 20. The width of the $a_0(1450)$ is relatively stable, and hence we quote $m = (1480 \pm 30) \text{ MeV}/c^2$ and $\Gamma = (265 \pm 15) \text{ MeV}/c^2$. This is the best fit that can be achieved with the channel $K_L K^\pm \pi^\mp$ only.

The intensity distribution of $\bar{K}K$ P wave produced from $^1S_0 \bar{p}p$ initial state [Fig. 5(c)] shows maxima at positions where the discrepancies in the Dalitz plot are observed. The form of the deviations is created by the interference with the $K^*(892)$ amplitudes and the $a_0(1450)$ amplitude. The data are rather insensitive to the intensity enhancement of the transition $\bar{p}p(^3S_1) \rightarrow \rho^\pm \pi^\mp; \rho^\pm \rightarrow K_L K^\pm$ [Fig. 5(i)] at high $K_L K^\pm$ masses. Information about the production of $\bar{K}K$ P wave from 3S_1 originates from all over the Dalitz plot area where it easily picks up some intensity from the likewise extended $K\pi$ S wave produced from 1S_0 .

IV. DISCUSSION

The production parameters for the best fit are compiled in Table I and the theoretical Dalitz plot is displayed in Fig. 9. The fit quality can be seen from the mass projections (Fig. 9) with the fitted intensity distribution superimposed on the data.

The fit requires about 60% contribution from 1S_0 and about 40% from 3S_1 initial states. It is instructive to compare

the production of the meson resonances with previous measurements. Our absolute branching ratios for decays into $\bar{K}K\pi$ are given in Table II and are normalized to Eq. (8).

The relative production of $K^*(892)\bar{K} \pm \bar{K}^*(892)K$ from 3S_1 to 1S_0 is $r = 3.0 \pm 0.6$ in agreement with the previous determination from Bettini *et al.* [19] $r = 2.4 \pm 0.5$. As in the bubble chamber experiment we have integrated the coherent sum of the K^* amplitude and its charge conjugate [19,16]. If the interference between the two K^* bands is neglected by integrating each $K^*(892)$ amplitude independently from the other one, slightly modified intensities are obtained. This causes, however, a drastic change to the contribution of the $K^*(1430)$ which extends over the whole Dalitz plot. Since destructive interference removes most of the wave produced from the $I=1$ initial state, one obtains a much higher intensity by integrating the two $K^*(1430)$ branches independently: instead of $(4.7 \pm 2.0)\%$ we get $2 \times (20.0 \pm 8.5)\%$. For the transition from the $I=0$ initial state we have individual contributions of $2 \times (7.8 \pm 1.8)\%$ instead of $(30.3 \pm 7.0)\%$. For broad objects the branching ratios are a matter of definition and should not, therefore, be taken at face value. The strong $K\pi$ S wave has already been noticed in Ref. [18]. In fact, from our observations [7] we expect annihilation from S states into any three pseudoscalars to proceed dominantly through two-body 0^{++} waves.

The intensity at the $\bar{K}K$ threshold is attributed to the $a_0(980)$, which we also observed [1] in the annihilation channel $\pi^0\pi^0\eta$ with a branching ratio of $B(\bar{p}p \rightarrow a_0(980)\pi; a_0 \rightarrow \pi\eta) = (2.61 \pm 0.48) \times 10^{-3}$. Since the resonance lies extremely close to the threshold of the $\bar{K}K$ channel, its apparent intensity distribution in $\bar{K}K$ and $\pi\eta$ is very much different from that of a Breit-Wigner resonance. Figure 10 shows its cusp-like shape for the $\pi\eta$ channel and in hatched style the intensity distribution in $\bar{K}K$, where $a_0(1450)$ is neglected. For this plot we have recalculated the Flatté amplitude F , Eq. (16), and corrected for two-body

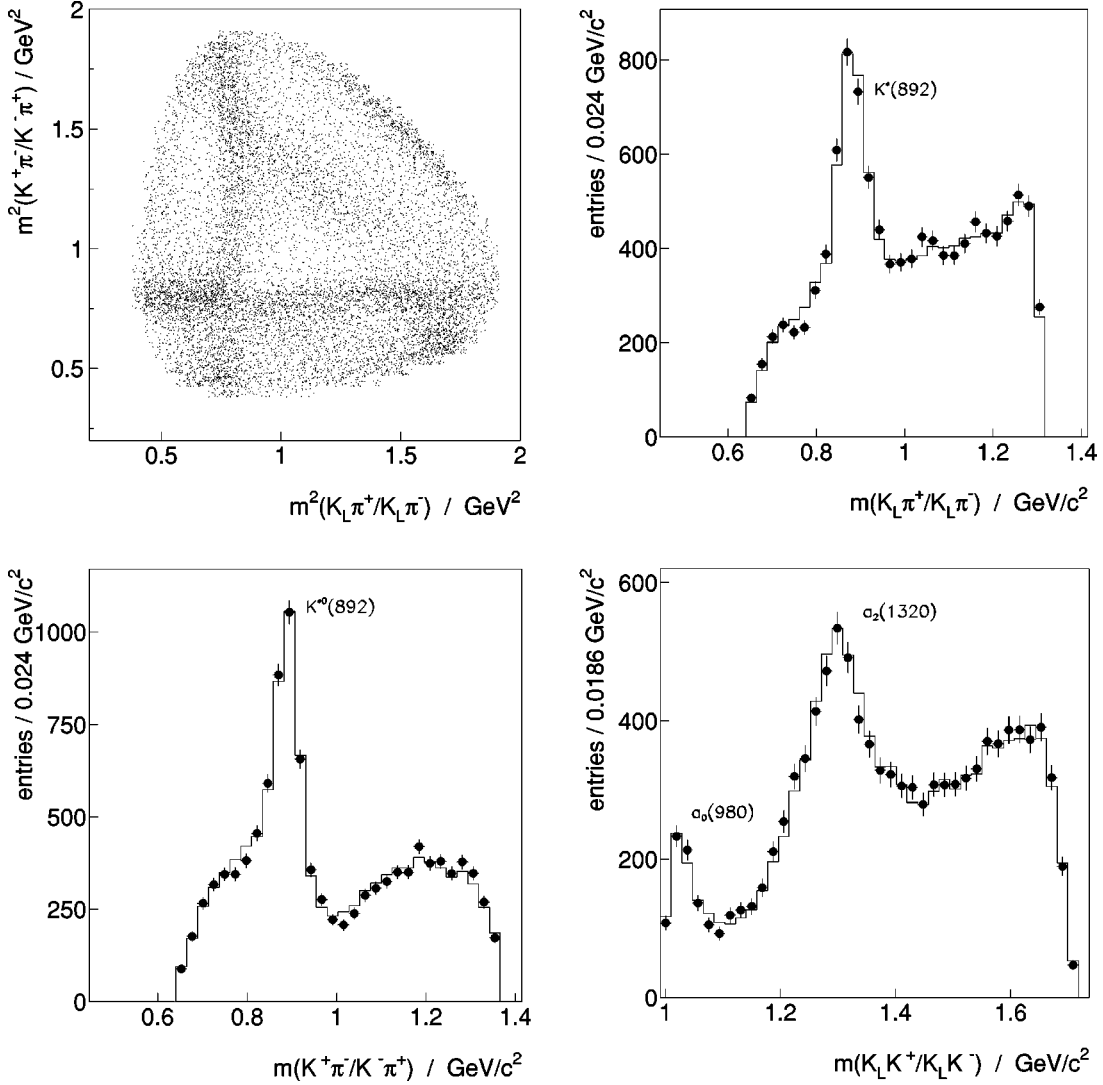


FIG. 9. Theoretical Dalitz plot corresponding to the best fit, and the mass projections with the fit (line) superimposed to the data (dots).

phase space. From Table II and Ref. [1] we calculate the ratio of branching ratios:

$$r(a_0(980)) = \frac{B(\bar{p}p \rightarrow a_0 \pi; a_0 \rightarrow \bar{K}K)}{B(\bar{p}p \rightarrow a_0 \pi; a_0 \rightarrow \pi\eta)} = 0.23 \pm 0.05. \quad (19)$$

The ratio of couplings to $\pi\eta$ and $\bar{K}K$ is extracted by fitting Eq. (16) with the constraint that the ratio of the integrated intensities is equal to our fit result Eq. (19). The K-matrix pole was determined in the Dalitz plot analysis to be $m_0 = (999 \pm 2)$ MeV/ c^2 and was fixed for this procedure. We obtain the coupling $g_{\pi\eta} = g_1 = 324 \pm 15$ MeV and a ratio of couplings $r = g_2^2/g_1^2 = 1.03 \pm 0.14$. This compares well with our estimate in Ref. [1] even though there we had to rely on the line shape to extract information about the $\bar{K}K$ partial width. In the present procedure the constraining information on the couplings is the number of events attributed to the $a_0(980)$ which is rather insensitive to the mass resolution. The pole positions in the complex energy plane corresponding to the parameters above are: in Riemann sheet II (m

TABLE II. Branching ratios of the meson resonances R contributing to $K_L K^\pm \pi^\mp$, calculated from the relative intensities in Table I and Eq. (8).

1S_0	$B(\bar{p}p \rightarrow R \pi \rightarrow \bar{K}K \pi) \times 10^4$	
$a_0(980)$		$5.92^{+0.46}_{-1.01}$
$a_0(1450)$		8.88 ± 1.68
$\bar{K}K$ P-wave		$1.75^{+0.28}_{-0.55}$
$a_2(1320)$		$12.00^{+0.93}_{-2.53}$
1S_0	$B(\bar{p}p \rightarrow RK \rightarrow \bar{K}K \pi) \times 10^4$	
$K^*(1430)$	$I_{\bar{p}p}^- = 0$	24.91 ± 5.83
	$I_{\bar{p}p}^- = 1$	3.86 ± 1.65
$K^*(892)$	$I_{\bar{p}p}^- = 0$	6.17 ± 0.85
	$I_{\bar{p}p}^- = 1$	0.90 ± 0.33
3S_1	$B(\bar{p}p \rightarrow R \pi \rightarrow \bar{K}K \pi) \times 10^4$	
$\bar{K}K$ P-wave		2.63 ± 0.83
$a_2(1320)$		2.85 ± 0.88
3S_1	$B(\bar{p}p \rightarrow RK \rightarrow \bar{K}K \pi) \times 10^4$	
$K^*(892)$	$I_{\bar{p}p}^- = 0$	4.52 ± 1.24
	$I_{\bar{p}p}^- = 1$	16.60 ± 2.54

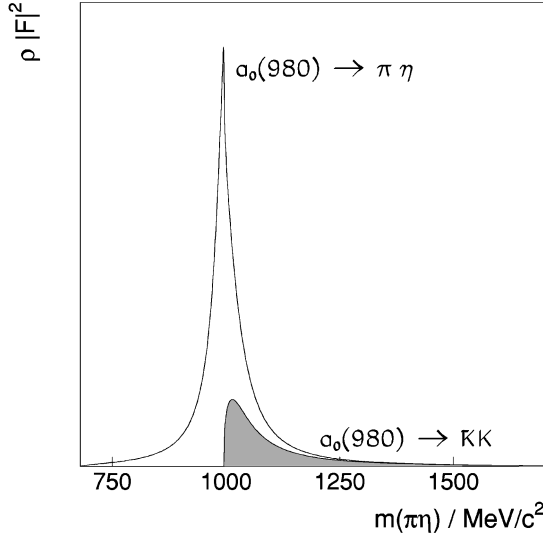


FIG. 10. Amplitudes $\rho_{\pi\eta}|F_{\pi\eta}|^2$ and $\rho_{\bar{K}K}|F_{\bar{K}K}|^2$ (shaded area).

$-i\Gamma/2) = (982 - i46) \text{ MeV}/c^2$ and in sheet III $(1006 - i49) \text{ MeV}/c^2$. The relevant value closest to the physical sheet for an object appearing as a resonance below the second threshold is sheet II, and hence we obtain a mass and a width for the $a_0(980)$, including the uncertainties from the underlying parameters: $m = 982 \pm 3 \text{ MeV}/c^2$ and $\Gamma = 92 \pm 8 \text{ MeV}/c^2$. The full width at half maximum of the $\pi\eta$ peak in Fig. 10 is $45 \text{ MeV}/c^2$, which is about half the resonance width.

We have introduced the $a_0(1450)$ into the same K matrix, but have not considered its coupling to the $\pi\eta$ channel, since it is far away from both thresholds. We have probed the significance of this resonance by fitting the Dalitz plot for fixed values of the $a_0(1450)$ contribution, leaving its mass and width at the values found for the best fit. The χ^2 dependence of the $a_0(1450)$ contribution is displayed in Fig. 11. For a contribution of 0.5% the $\Delta\chi^2$ reaches 100; if $a_0(1450)$ is omitted $\Delta\chi^2 = 150$.

From SU(3)-flavor symmetry assuming that $a_0(1450)$ is the $\bar{q}q$ octet state and the relative creation of $\bar{u}u$ or $\bar{d}d$ versus

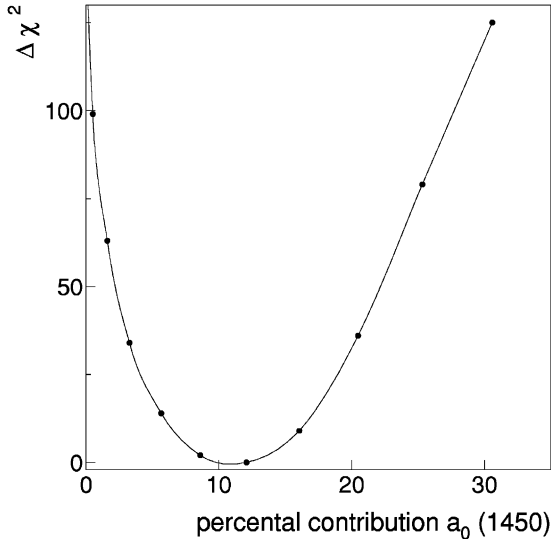


FIG. 11. χ^2 scan for different intensities of $a_0(1450)$.

$\bar{s}s$ is equally probable, we predict the relative coupling of the $a_0(1450)$ to $\bar{K}K$ and $\pi\eta$:

$$r_1(a_0(1450)) = \frac{B(a_0 \rightarrow \bar{K}K)}{B(a_0 \rightarrow \pi\eta)} = \frac{1}{2 \cos^2 \phi} \frac{q_{\bar{K}K}}{q_{\pi\eta}}, \quad (20)$$

where $\phi = 54.7^\circ + \theta_{PS}$. With a pseudoscalar mixing angle from Ref. [32] of $\theta_{PS} = -(17.3 \pm 1.8)^\circ$ and phase space evaluated at $m = 1480 \text{ MeV}/c^2$ we obtain:

$$r_1(a_0(1450)) = 0.69 \pm 0.03. \quad (21)$$

The error is determined by the uncertainty in the pseudoscalar mixing angle. With the branching ratio $B(\bar{p}p \rightarrow a_0\pi; a_0 \rightarrow \pi\eta) = (10.05 \pm 1.80) \times 10^{-4}$ from Ref. [1] we obtain

$$r_1(a_0(1450)) = 0.88 \pm 0.23, \quad (22)$$

which agrees with Eq. (21). Recently, we also published the branching ratio for the $\pi^0\eta'$ decay of this resonance extracted from the partial wave analysis of the final state $\pi^0\pi^0\eta'$ of $\bar{p}p$ annihilation at rest [2]. Summarizing, we find the following ratios of branching ratios compared to flavor SU(3):

	$\pi\eta$	$\bar{K}K$	$\pi\eta'$
SU(3)	1.	0.69 ± 0.03	0.39 ± 0.04
Crystal Barrel	1.	0.88 ± 0.23	0.35 ± 0.16

The isovector scalar resonance $a_0(1450)$ is well described by the decay pattern predicted by flavor SU(3). Hence, it naturally finds its place in the 0^{++} nonet.

We now compare the branching ratio of $a_2(1320)$, $B(\bar{p}p(^1S_0, ^3S_1) \rightarrow a_2\pi; a_2 \rightarrow \bar{K}K) = (14.85 \pm 1.94) \times 10^{-4}$ from this analysis with the value from bubble chamber work $B = (12.4 \pm 1.9) \times 10^{-4}$ [19]. There the $a_2(1320)$ mass was found below 1300 MeV. We explain this mass shift by the interference with $a_0(1450)$. For the ratio of $a_2(1320)$ production from the initial states 1S_0 and 3S_1 we get

$$f = \frac{B(\bar{p}p(^1S_0) \rightarrow a_2\pi)}{B(\bar{p}p(^3S_1) \rightarrow a_2\pi)} = 4.2_{-1.6}^{+1.3}, \quad (23)$$

compared to $f = 3.0 \pm 1.5$ from Ref. [18]. However, we do not attach much significance to this agreement because of the large errors. The relative decay ratio of $a_2(1320)$ from the present analysis and the $\pi^0\pi^0\eta$ result [1] $B(\bar{p}p(^1S_0) \rightarrow a_2(1320)\pi^0; a_2(1320) \rightarrow \pi^0\eta) = (1.9 \pm 0.3) \times 10^{-3}$ is

$$r_1(a_2(1320)) = \frac{B(a_2 \rightarrow \bar{K}K)}{B(a_2 \rightarrow \pi\eta)} = 0.21_{-0.06}^{+0.04}. \quad (24)$$

PDG [20] quote $r_1(a_2(1320)) = 0.34 \pm 0.06$. In the recent analysis of the reaction $\bar{p}p \rightarrow \pi^0\pi^0\eta'$ [2] we found $B(\bar{p}p(^1S_0) \rightarrow a_2(1320)\pi^0; a_2 \rightarrow \pi^0\eta') = (6.4 \pm 1.3) \times 10^{-5}$, which gives a relative decay ratio:

$$r_2(a_2(1320)) = \frac{B(a_2 \rightarrow \pi\eta')}{B(a_2 \rightarrow \pi\eta)} = 0.034 \pm 0.009, \quad (25)$$

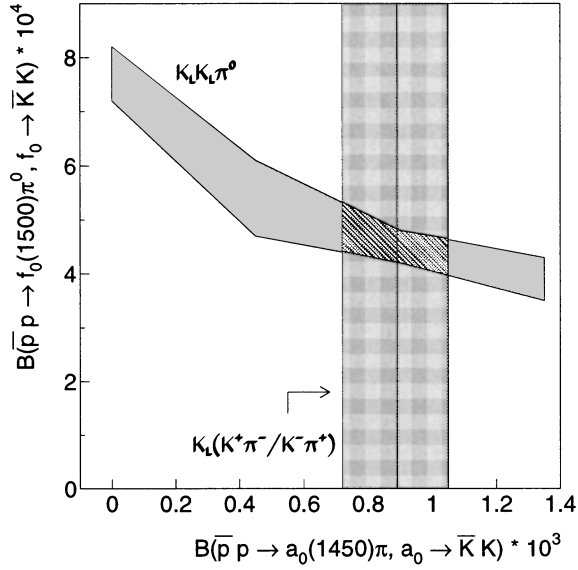


FIG. 12. Determination of the branching ratio of $f_0(1500)$ in the reaction $\bar{p}p \rightarrow K_L K_L \pi^0$ [9] (light hatched area), where it is correlated with $a_0(1450)$ production. The $a_0(1450)$ contribution is fixed by the present measurement (dark hatched area).

while PDG gives $r_2(a_2(1320)) = 0.039 \pm 0.008$. Both agree.

Let us now discuss the impact of the present analysis on the interpretation of the $I=0$ scalar resonance $f_0(1500)$, which we have observed earlier in different final states of $\bar{p}p$ annihilation from 1S_0 . It was found [9] that the $f_0(1500)$ contribution to the final state $K_L K_L \pi^0$ of $\bar{p}p$ annihilation at rest depends on the contribution of $a_0(1450)$ (see Fig. 12). We can now eliminate this correlation using Eq. (1). The branching ratio for $f_0(1500)$ is determined to be $B(\bar{p}p \rightarrow f_0(1500) \pi; f_0(1500) \rightarrow \bar{K}K) = (4.52 \pm 0.36) \times 10^{-4}$. SU(3) flavor symmetry predicts for a pure $\bar{s}s$ meson a coupling of $\bar{K}K$ relative to $\pi\pi$ of $r = \infty$ and for a $(\bar{u}u + \bar{d}d)$ meson $r = \frac{1}{3}$. With $B(\bar{p}p \rightarrow f_0(1500) \pi; f_0(1500) \rightarrow \pi^0 \pi^0) = (8.1 \pm 2.8) \times 10^{-4}$ from Ref. [3] we calculate

$$r = \frac{B(f_0 \rightarrow \bar{K}K) q_{\pi\pi}}{B(f_0 \rightarrow \pi\pi) q_{\bar{K}K}} = 0.24 \pm 0.09. \quad (26)$$

Using the coupled channel analysis [7] leads to a slightly smaller but consistent value $r = 0.16 \pm 0.04$. Ratio (26) makes the interpretation of $f_0(1500)$ as $\bar{s}s$ meson rather unlikely. Its decay branching ratios are similar to those of a $(\bar{u}u + \bar{d}d)$ meson. The scalar nonet can be constructed from Crystal Barrel investigations with $f_0(1370)(I=0)$, $a_0(1450)(I=1)$ and $K^*(1430)(I=\frac{1}{2})$ as in Ref. [33]. The position of the ω -like partner of a nonet is already occupied by $f_0(1370)$. The supernumerary status of $f_0(1500)$ is supported by its small width compared to the nonet members [34,35]. The glueball interpretation of the $f_0(1500)$ based on its couplings is discussed in Refs. [36, 37]. According to these calculations the ϕ -like scalar meson has to be found at masses above $1600 \text{ MeV}/c^2$.

V. CONCLUSIONS

We have measured the $K_L K^\pm \pi^\mp$ final state of $\bar{p}p$ annihilation at rest with five times more statistics than previous bubble chamber experiments. We established the $\bar{K}K$ decay mode of $a_0(1450)$ by a partial wave analysis in the isobar model and formulated the dynamics in the K-matrix formalism. The branching ratio is $B(\bar{p}p \rightarrow a_0(1450) \pi; a_0(1450) \rightarrow \bar{K}K) = (8.88 \pm 1.68) \times 10^{-4}$. The mass and width are $m = 1480 \pm 30 \text{ MeV}/c^2$ and $\Gamma = 265 \pm 15 \text{ MeV}/c^2$, respectively. We were also able to determine the branching ratio for $f_0(1500)$: $B(\bar{p}p \rightarrow \pi f_0(1500); f_0(1500) \rightarrow \bar{K}K) = (4.52 \pm 0.36) \times 10^{-4}$.

ACKNOWLEDGMENTS

We would like to thank the technical staff of the LEAR machine group and of all the participating institutions for their invaluable contributions to the success of the experiment. We acknowledge financial support from the German Bundesministerium für Bildung, Wissenschaft, Forschung und Technologie, the Schweizerischer Nationalfonds, the British Particle Physics and Astronomy Research Council, the U.S. Department of Energy and the National Science Research Fund Committee of Hungary (contract No. DE-FG03-87ER40323, DE-AC03-76SF00098, DE-FG02-87ER40315 and OTKA T023635). K. M. Crowe and F.-H. Heinsius acknowledge support from the A. von Humboldt Foundation, and N. Djaoshvili from the DAAD.

[1] C. Amsler *et al.*, Phys. Lett. B **333**, 277 (1994).
 [2] A. Abele *et al.*, Phys. Lett. B **404**, 179 (1997).
 [3] C. Amsler *et al.*, Phys. Lett. B **342**, 433 (1995).
 [4] C. Amsler *et al.*, Phys. Lett. B **353**, 571 (1995).
 [5] C. Amsler *et al.*, Phys. Lett. B **340**, 259 (1994).
 [6] A. Abele *et al.*, Phys. Lett. B **380**, 453 (1996).
 [7] C. Amsler *et al.*, Phys. Lett. B **355**, 425 (1995).
 [8] G. S. Bali *et al.*, Phys. Lett. B **309**, 378 (1993); J. C. Sexton *et al.*, Phys. Rev. Lett. **75**, 4563 (1995).
 [9] A. Abele *et al.*, Phys. Lett. B **385**, 425 (1996).
 [10] E. Aker *et al.*, Nucl. Instrum. Methods Phys. Res. A **321**, 69 (1992).
 [11] M. Heinzelmann, Diploma thesis, University Zürich, 1996.

[12] GEANT, CERN Program Library long writeup W5013.
 [13] P. A. Aarnio *et al.*, Fluka users guide, Technical report TIS-RP-190, CERN, 1990.
 [14] O. Cramer, Diploma thesis, University Munich, 1993.
 [15] R. Armenteros *et al.*, Phys. Lett. **17**, 170 (1965).
 [16] N. Barash *et al.*, Phys. Rev. **139**, B1659 (1965).
 [17] C. Amsler and F. Myhrer, Low Energy Antiproton Physics, CERN-PPE/91-29(1991).
 [18] B. Conforto *et al.*, Nucl. Phys. **B3**, 469 (1967).
 [19] A. Bettini *et al.*, Nuovo Cimento A **78**, 1199 (1969).
 [20] Particle Data Group, R. M. Barnett *et al.*, Phys. Rev. D **54**, 1 (1996).
 [21] C. J. Batty, Nucl. Phys. **A601**, 425 (1996).

- [22] C. Amsler and J. C. Bizot, *Comput. Phys. Commun.* **30**, 21 (1983).
- [23] C. Amsler *et al.*, *Z. Phys. C* **58**, 175 (1993).
- [24] S. U. Chung *et al.*, *Ann. Phys. (N.Y.)* **4**, 404 (1995).
- [25] F. James and M. Roos, CERN Library long writeup D506, 1987.
- [26] S. Baker and R. D. Cousins, *Nucl. Instrum. Methods Phys. Res. A* **221**, 437 (1984).
- [27] S. M. Flatté, *Phys. Lett.* **63B**, 224 (1976).
- [28] S. Spanier, Ph.D. thesis, University Mainz, 1994.
- [29] D. Aston *et al.*, *Nucl. Phys.* **B296**, 491 (1988).
- [30] W. E. Cleland *et al.*, *Nucl. Phys.* **B208**, 228 (1982).
- [31] A. Abele *et al.*, *Phys. Lett. B* **391**, 191 (1997).
- [32] C. Amsler *et al.*, *Z. Phys. C* **42**, 175 (1993).
- [33] S. Spanier, in *QCD 96*, Proceedings of the Conference, Montpellier, France, 1996, edited by S. Narison [*Nucl. Phys. B (Proc. Suppl.)* **54A**, 362 (1997)].
- [34] S. Godfrey and N. Isgur, *Phys. Rev. D* **32**, 189 (1985).
- [35] R. Kokoski and N. Isgur, *Phys. Rev. D* **35**, 907 (1987).
- [36] C. Amsler and F. E. Close, *Phys. Rev. D* **53**, 295 (1996).
- [37] F. E. Close, G. R. Farrar, and Z. Li, *Phys. Rev. D* **55**, 5749 (1997).